Enhancement of Coastline Video Monitoring System Using Structuring Element Morphological Operations

I Gusti Ngurah Agung Pawana[1], I Made Oka Widyantara[2],
Made Sudarma[3], Dewa Made Wiharta[4], Made Widya Jayantari[5]
Electrical Engineering Department, Udayana University, Badung, Indonesia[1, 2, 3, 4]
Civil Engineering Department, Udayana University, Badung, Indonesia[5]

***Abstract*—Coastal monitoring is vital in environmental management, disaster mitigation, and addressing climate change impacts. Traditional methods are time-consuming and error-prone, prompting the need for innovative systems. This study introduces the Coastal Video Monitoring System (CoViMos), a novel framework for real-time shoreline detection in tropical regions, specifically at Kedonganan Beach, Bali. The CoViMos framework utilizes advanced video monitoring and optimized morphological operations to address challenges such as environmental noise and dynamic shoreline behavior. Key innovations include Kapur's entropy thresholding enhanced with the Grasshopper Optimization Algorithm (GOA) and structuring elements tailored to the beach's unique features. Sensitivity analysis reveals that a structuring element size of five pixels offers optimal performance, balancing efficiency, and image fidelity. This configuration achieves peak values in quality metrics such as the Peak Signal-to-Noise Ratio (PSNR), Structural Similarity Index (SSIM), Complex Wavelet SSIM (CWSSIM), and Feature Similarity Index (FSIM) while minimizing Mean Squared Error (MSE) and reducing processing time. The results demonstrate significant improvements in shoreline detection accuracy, with PSNR increasing by 9.3%, SSIM by 1.4%, CWSSIM by 1.7%, and FSIM by 1.6%. Processing time decreased by 1.3%, emphasizing the system's computational efficiency. These enhancements ensure more precise shoreline mapping, even in noisy and dynamic environments.**

***Keywords*—Coastline detection; image processing; Video Monitoring System (CoViMoS); morphological operations**

I. Introduction

Coastal monitoring plays a critical role in environmental management, disaster preparedness, and marine resource protection [1], [2], [3]. Effective monitoring systems rely heavily on accurately detecting and analyzing coastal lines, which are inherently dynamic due to erosion, tidal variations, and climate change. Traditional methods of coastline monitoring involve manual interpretation of satellite images and field surveys, which are time-consuming, prone to human error, and less effective in real-time scenarios [4], [5]. These limitations necessitate automated and robust systems that leverage advanced image processing techniques for accurate coastline detection.

Kedonganan Beach in Bali is a complex and dynamic ecosystem shaped by natural forces like tides, waves, sediment deposition, and human activities, including tourism, fishing, and urban development. Effective shoreline detection and monitoring are critical for sustainable coastal management, disaster mitigation, and environmental preservation. However, accurate shoreline detection presents significant challenges due to the dynamic and irregular nature of tropical coastlines, ecological noise (e.g., glare, wave foam, or debris), and the limitations of existing image processing techniques [6], [7]. Addressing these challenges requires an innovative and adaptive approach that can handle the unique complexities of coastal environments.

To overcome these challenges, this research introduces a novel framework called the Coastal Video Monitoring System (CoViMos), specifically designed to monitor and analyze shoreline dynamics in tropical coastal areas. The CoViMos framework utilizes video monitoring as its foundation, enabling continuous visual data capture over time. Unlike traditional static image-based approaches, CoViMos offers dynamic and real-time insights into shoreline behavior, making it particularly useful for understanding the effects of seasonal changes, storm events, and anthropogenic activities on the shoreline. This framework serves as the backbone of the methodology, facilitating the acquisition, preprocessing, and segmentation of coastal imagery to detect and map the shoreline accurately.

Recent advancements in image processing have focused on enhancing feature extraction using techniques like edge detection, segmentation, and morphological operations [8], [9], [10]. The Canny Edge Detector, for instance, is widely recognized for its ability to detect edges with minimal noise. Still, its effectiveness diminishes in noisy and low-contrast environments common in coastal imagery. Morphological operations, particularly when utilizing structuring elements, have shown promise in addressing these challenges by refining edges, enhancing feature continuity, and suppressing noise. However, existing research primarily focuses on static image datasets, leaving a gap in the context of real-time video monitoring systems for dynamic coastal environments. Additionally, there is limited exploration of optimal structuring element configurations, such as size and shape, to balance signal quality, structural similarity, and computational efficiency.

The post-segmentation process in this study plays a pivotal role in refining the results obtained from CoViMos. Segmentation isolates the shoreline from other features in coastal imagery, such as wave crests, foam, and reflections, which can often distort detection accuracy. Following the segmentation process, post-processing techniques are applied to clean up noise and enhance the delineation of the shoreline boundary. This step ensures that the detected shoreline

accurately represents the true physical boundary between land and water, even under challenging conditions like high tidal activity or environmental noise.

Studies by Kaur and Singh [11] demonstrate the potential of structuring elements in improving the Peak Signal-to-Noise Ratio (PSNR) and Structural Similarity Index (SSIM). However, their focus has been largely theoretical, lacking practical application to real-world dynamic systems like coastline monitoring. This research addresses these gaps by integrating structuring element morphological operations into a real-time video monitoring framework and conducting a comprehensive sensitivity analysis of structuring element configurations.

A major innovation of this research lies in enhancing morphological operations during the post-segmentation process. Morphological operations, such as dilation and erosion, are widely used in image processing to refine object boundaries [12], [13], [14]. However, traditional approaches often rely on generic structural elements, such as rectangular or circular shapes, which are inadequate for capturing tropical shorelines' irregular and dynamic patterns. In this study, a tailored structural element morphology is developed to address these limitations. These structural elements are designed based on the specific characteristics of Kedonganan Beach, considering the curvature of waves, sedimentary features, vegetation interference, and other coastal-specific patterns. By optimizing the shape, size, and orientation of the structural elements, the proposed methodology significantly improves the accuracy of morphological operations, enabling more precise shoreline detection.

The CoViMos framework, combined with optimized post-segmentation processes and advanced structural element morphology, offers a comprehensive solution to the challenges of shoreline detection in tropical coastal environments. This research's contribution lies in its ability to enhance the robustness and precision of shoreline mapping, even in the presence of high environmental variability and noise. Furthermore, the novelty of the tailored structural elements provides a scalable approach that can be adapted to other coastal regions with similar complexities.

By addressing existing gaps in traditional shoreline detection methods, this study advances the state of the art in coastal monitoring technologies and provides practical benefits for coastal management. The insights derived from the improved shoreline detection process can be used to support decision-making in areas such as erosion control, habitat conservation, and disaster risk reduction. Ultimately, integrating the CoViMos framework and innovations in morphological operations will contribute to developing a reliable and adaptive tool for sustainable coastal management, focusing on tropical regions like Kedonganan Beach.

II. Research Methods

A. Study Area

Kedonganan Beach, located in southern Bali, Indonesia, is a renowned coastal area known for its pristine beauty, vibrant seafood market, and traditional fishing activities. The beach, part of Bali's western coastline along the Indian Ocean, holds significant cultural and economic importance due to its role as a tourist hotspot and a hub for local livelihoods. Its sandy shores, shallow waters, and adjacent coastal vegetation make it a dynamic environment influenced by natural processes like tides, wave actions, seasonal weather patterns, and human activities such as urban development and tourism infrastructure.

Research on coastline detection at Kedonganan Beach is crucial for several reasons. The area is prone to coastal erosion and accretion, and understanding these changes is vital for sustainable coastal management. Accurate mapping of the coastline supports the preservation of the beach's aesthetic appeal, which is essential for tourism, and helps ensure the stability of local fishing activities.

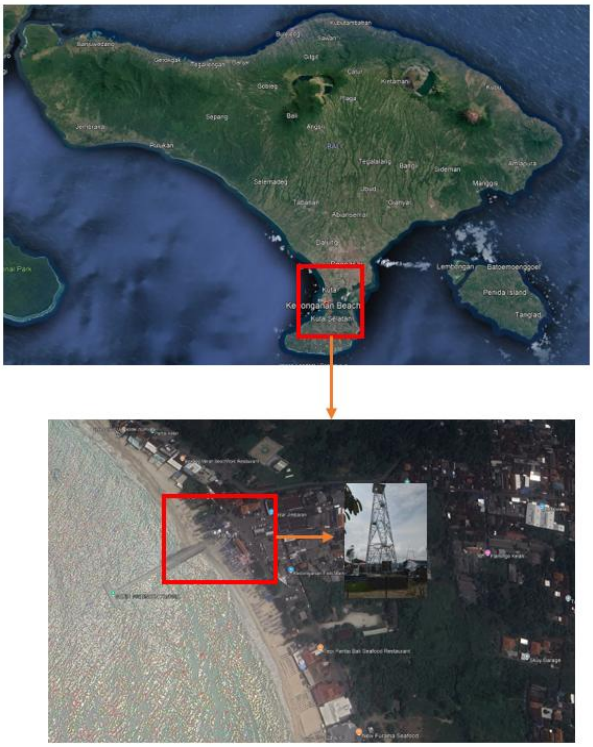

Fig. 1. Study area.

B. Research Data and Tools

The dataset used in this study is derived from camera video monitoring data captured in the Kedonganan tower, as seen in Fig. 1. The time-exposure method converts the video data into images using MATLAB. The camera's specifications are in Table I.

TABLE I. Camera Specification

Specifications	
Model	CS-EB8 (3MP,4GA)
Lens	Viewing angle: 100° (Diagonal), 83° (Horizontal), 44° (Vertical)
Max Resolution	2304 x 1296
Frame Rate	Max. 15fps; Self-Adaptive during network transmission
Video Compression	H.265 / H.264

C. Coastline Video Monitoring System Framework (CoViMoS)

The CoViMos framework (Fig. 2) begins with acquiring coastal video footage, a widely used tool for shoreline monitoring due to its ability to capture temporal changes in shoreline position [15]. Coastal videos provide continuous spatial coverage and are suitable for extracting shoreline positions in dynamic coastal environments [16]. The video frames are pre-processed to generate composite images, such as time-averaged (Timex) images, that minimize noise from transient waves.

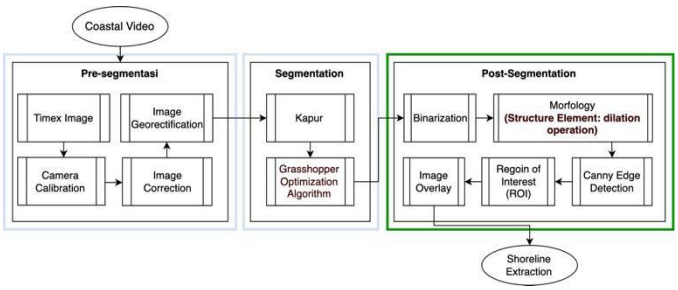

Fig. 2. CoViMos framework.

1) Pre-Segmentation: The video frames are processed in this phase to improve image quality and align them with real-world spatial references. Timex images are generated to create a stable representation of coastal features, removing the effects of wave activity. Camera calibration ensures geometric accuracy by correcting lens distortions, while image correction adjusts brightness, contrast, and noise for improved clarity. Lastly, image georectification aligns the image with geographic coordinates, enabling precise spatial analysis [15].

2) Segmentation: Segmentation identifies the shoreline by separating the foreground (shoreline) and background (sea or land). Kapur's entropy-based thresholding is widely used in image processing, as it maximizes inter-class variance based on pixel intensity distributions [17], [18], [19]. The Grasshopper Optimization Algorithm (GOA) is employed to enhance threshold optimization. GOA is inspired by swarm intelligence and has demonstrated robust performance in solving complex optimization problems in image processing [20], [21], [22]. This step ensures accurate shoreline delineation by optimizing the thresholds derived from Kapur's method.

3) Post-Segmentation: Post-segmentation refines the results by applying advanced image processing techniques. Binarization converts the segmented image into a binary format for clarity. Morphological operations, such as dilation, fill gaps and enhance connectivity in the segmented shoreline. The Canny edge detection algorithm detects firm edges, often indicative of shoreline boundaries [23], [24], [25]. Additionally, the Region of Interest (ROI) is defined as focusing on areas where shoreline features are most prominent, reducing noise from irrelevant regions.

4) Shoreline extraction: The final shoreline is extracted by combining the outputs from segmentation and post-segmentation. Binary and morphology-processed images ensure a well-defined shoreline, while edge detection sharpens the boundary. The extracted shoreline can be visually validated and used for further analysis by overlaying the ROI on the original image.

5) Enhancement of coastline video monitoring system Framework Using Structuring Element Morphological Operations.

Morphological operations, such as dilation, are applied to the binary image to refine its features. Dilation, which uses a structuring element (SE), expands the boundaries of foreground objects, bridging gaps and filling small holes. This process is beneficial for connecting fragmented coastline features that may arise due to noise or irregularities in the segmented image. Devkota et al. [26] emphasize that morphological operations enhance the shape and structure of binary objects in image analysis. By using an appropriate SE, dilation ensures that the coastline features are continuous and prominent, enabling more accurate detection in subsequent steps (Fig. 3).

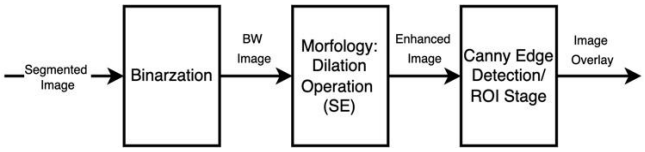

Fig. 3. Flowchart (Coastline features).

Enhancing coastline video monitoring systems using structuring element morphological operations offers several benefits, particularly for improving detection accuracy and handling complex environments. These operations, such as dilation, erosion, and the morphological gradient, refine image edges and contours by removing noise, filling gaps, and enhancing the continuity of detected lines. This is especially crucial in coastal settings where irregular patterns arise due to tides, vegetation, and human activities. Moreover, the lightweight computational nature of morphological operations makes them suitable for real-time processing, enabling dynamic monitoring of changing coastal conditions. These operations ensure more precise and reliable line detection by reducing environmental noise, such as reflections from water surfaces or shadows. They can also be effectively integrated with advanced image processing techniques, like edge detection algorithms (e.g., Sobel, Canny) and machine learning models, to enhance their performance further [27], [28]. Scientific literature highlights the benefits of morphological operations in edge detection and image analysis.

D. Performance Analysis of Coastline Video Monitoring Systems

The Performance Analysis of Coastline Video Monitoring Systems involves evaluating the system's ability to accurately detect shorelines and assess video quality through several key performance metrics. The Peak Signal-to-Noise Ratio (PSNR) measures the quality of the detected shoreline by comparing the detected video to the ground truth, where higher PSNR values indicate less noise and better preservation of the original shoreline. The Structural Similarity Index (SSIM) provides a more perceptually accurate measure of image quality by assessing the similarity in structural elements such as luminance, contrast, and texture between the detected and ground truth

images. For further accuracy, the Complex Wavelet SSIM (CW-SSIM) incorporates wavelet transforms, making it robust against small distortions and shifts in video frames, allowing for a more detailed evaluation of shoreline detection. The Feature Similarity Index Measure (FSIM) also focuses on low-level image features like phase congruency and gradient magnitude, offering an in-depth analysis of how well the system preserves critical shoreline features. Lastly, the Execution Time metric assesses the system's processing speed, which is crucial for applications requiring real-time or near-real-time performance.

PSNR measures the ratio between a signal's maximum possible power and noise's power. Higher PSNR indicates better quality. PSNR equation is shown in Eq. (1).

$$PSNR = 10 - \log_{10}\left(\frac{MAX^2}{MSE}\right) \quad (1)$$

Where:

- MAX is the maximum pixel intensity value (e.g., 255 for 8-bit images).
- MSE is the Mean Squared Error between the detected and ground truth shorelines. The MSE equation is shown in Eq. (2).

$$MSE = \frac{1}{N}\sum_{i=1}^{N}(X_i - Y_i)^2 \quad (2)$$

Xi and Yi are pixel intensities at location in the detected and ground truth images.

FSIM assesses similarity based on low-level features like phase congruency (PC) and gradient magnitude (GM). FSIM equation shown in Eq. (3).

$$FSIM = (x, y) = \frac{\sum_i PC_i \cdot S_{GM}(x_i, y_i)}{\sum_i PC_i} \quad (3)$$

Where:

- $\sum_i PC_i$ Is phase congruency at pixel i.
- $S_{GM}(x_i, y_i)$ Is gradient magnitude similarity at pixel i.

SSIM measures the structural similarity between two images. It is defined as Eq. (4).

$$SSIM(x, y) = \frac{(2\mu_x\mu_y + C_1)(2\sigma_{xy} + C_2)}{(\mu_x^2 + \mu_y^2 + C_1)(\sigma_x^2 + \sigma_y^2 + C_2)} \quad (4)$$

Where:

- μ_x, μ_y is the mean intensities of x and y.
- σ_x^2, σ_y^2 is variances of x and y.
- σ_{xy} is covariance of x and y.
- C_1, C_2 are small constants to stabilize the division.

CW-SSIM compares two images in the wavelet domain, providing robustness to small translations and distortions. The equation is shown in Eq. (5).

$$CW - SSIM(x, y) = \frac{|\sum_k x_y \cdot \bar{y}_{\bar{k}}|}{\sqrt{\sum_k |x_k|^2 \cdot \sum_k |y_k|^2}} \quad (5)$$

Where:

- x_y, y_k Are complex wavelet coefficients of the two images
- $\bar{y}_{\bar{k}}$ Is conjugate of y_k

III. Result and Discussion

A. Sensitivity Analysis in Structure Element Morphology Operation

Sensitivity analysis aims to evaluate how variations in specific features of the structuring element by pixel configuration changes impact morphological operations' outcomes. This process seeks to assess robustness by comparing the performance of the morphological operation under various configurations across multiple images. For this analysis, five trials were conducted using structuring elements of five different line lengths that are 2, 4, 5, 10, 15.

1) Peak Signal-to-Noise Ratio (PSNR): Fig. 4 shows the relationship between Peak Signal-to-Noise Ratio (PSNR) and pixel values, showcasing a decline in PSNR as pixel values increase. PSNR, commonly measured in decibels (dB), is a standard metric used to evaluate the quality of image reconstruction or compression by quantifying the similarity between an original and a distorted image. Higher PSNR values typically indicate better image quality. According to the data presented, the PSNR reaches its maximum value of 27.0245 dB at pixel 5, while the lowest value, 21.9970 dB, occurs at pixel 20. This trend aligns with findings in the literature, where an increase in pixel distortion or noise levels is often associated with a decline in PSNR, as documented by Elat et al. [29]. Such behavior highlights the sensitivity of PSNR to variations in noise and distortion, which is crucial in applications such as image compression, denoising algorithms, and watermarking. Additionally, the drop in PSNR with increasing pixel values underscores the trade-off between data modification and image quality, a phenomenon explored extensively in studies on adaptive filtering [30].

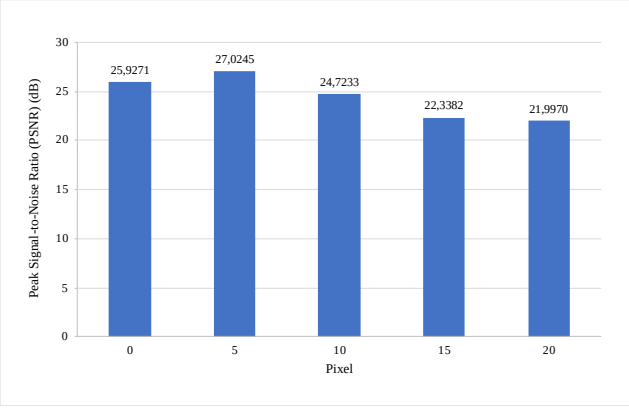

Fig. 4. Peak Signal-to-Noise Ratio (PSNR).

2) Mean Square Error (MSE): Fig. 5 shows the Mean Squared Error (MSE) values for various pixel levels, showcasing the relationship between pixel modifications and image distortion. MSE, a metric used to quantify the average

squared difference between the original and distorted image, increases as the level of distortion rises. At pixel 0, the MSE is 166.0989, which decreases to its lowest value of 129.0117 at pixel 5, indicating minimal error. However, as pixel values increase, the MSE rises significantly to 219.1567 at pixel 10, 379.5442 at pixel 15, and reaches its maximum of 410.5653 at pixel 20. This trend demonstrates that greater pixel variations result in higher distortion levels, as reflected by the increase in MSE. These findings align with established principles in image processing, where MSE effectively measures degradation, making it a critical tool for evaluating image quality and the impact of noise or modifications.

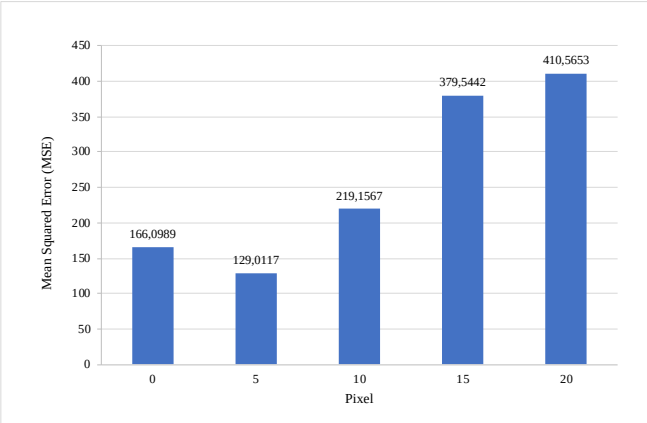

Fig. 5. Mean Square Error (MSE).

This trend indicates that the structural element size significantly impacts the error, with excessively small or large elements introducing more inaccuracies. The structural element of 5 pixels offers the best balance, minimizing error while maintaining quality. Such insights are critical in fields like image processing, where optimizing structural element size is essential for tasks like filtering, reconstruction, or morphological operations.

3) Structural Similarity Index (SSIM): Fig. 6 shows the relationship between the Structural Similarity Index (SSIM) and pixel values, highlighting the effect of pixel variations on image quality. SSIM, a widely used metric for evaluating image quality by measuring structural similarity, ranges from 0 to 1, with values closer to 1 indicating higher similarity. According to the data, the SSIM value peaks at 0.9171 for pixel 5, indicating the highest image quality. At pixel 0, the SSIM is 0.9138, slightly lower than the maximum. However, as pixel values increase, the SSIM steadily decreases, dropping to 0.9044 at pixel 10, 0.8782 at pixel 15, and the lowest value, 0.8646, at pixel 20. This trend aligns with findings in image processing literature, where higher noise or pixel alterations typically reduce structural similarity, resulting in a perceptible degradation of image quality. Such analysis highlights the sensitivity of SSIM to changes in pixel values, reinforcing its importance as a robust metric for evaluating image fidelity.

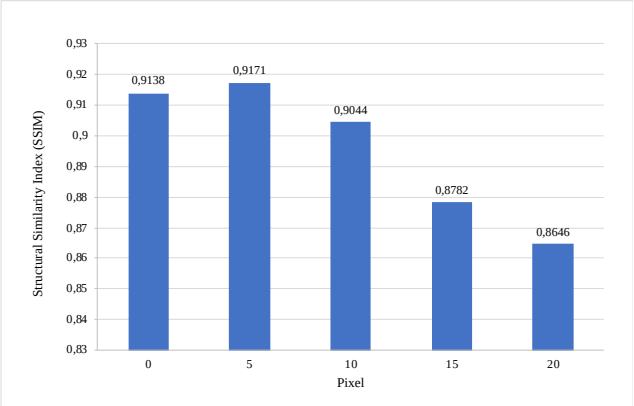

Fig. 6. Structural Similarity Index (SSIM).

4) Complex Wavelet Structural Similarity Index (CWSSIM): Fig. 7 shows the relationship between the Complex Wavelet Structural Similarity Index (CWSSIM) and varying pixel perturbation levels. CWSSIM, a metric designed to evaluate structural similarity in images or signals, shows a noticeable trend: as the pixel perturbation increases, the CWSSIM values decline, indicating reduced structural similarity between the reference and perturbed data. The CWSSIM is highest at 5 pixels (0.9749), reflecting maximum structural similarity, but progressively decreases, reaching its lowest value of 0.8159 at 20 pixels. This demonstrates the metric's sensitivity to structural changes caused by pixel perturbation.

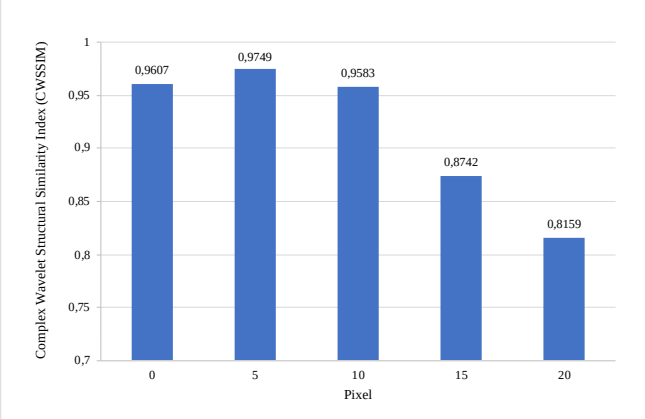

Fig. 7. Structural Similarity Index (CWSSIM).

The behavior observed in the graph aligns with findings in the literature. Yan et al. [31] introduced the Structural Similarity Index (SSIM) to measure perceptual image quality based on luminance, contrast, and structure. CWSSIM extends this approach into the wavelet domain, enabling it to capture structural variations effectively at multiple resolutions. Zhang [32] highlighted that wavelet-based similarity indices like CWSSIM are highly responsive to image distortions and offer robust mechanisms for analyzing localized changes. Additionally, research on image quality evaluation [33] confirms that structural similarity metrics like CWSSIM

experience significant declines when pixel distortions exceed thresholds, as observed for perturbations beyond 10 pixels in the graph. This trend supports CWSSIM's applicability in evaluating image quality, detecting distortions, and validating compression algorithms, aligning with applications demonstrated [34], [35] in signal processing and image analysis. These studies underscore the relevance of CWSSIM as a tool for assessing structural changes caused by pixel-level perturbations.

5) Feature Similarity Index (FSIM): Fig. 8 shows the relationship between pixel values and the Feature Similarity Index (FSIM), a metric used to measure image similarity, where higher values indicate greater similarity. The X-axis represents pixel values ranging from 0 to 20, while the Y-axis shows FSIM values ranging from 0.76 to 0.98. At 0 pixels, the FSIM is 0.9513, slightly increasing to 0.9547 at 5 pixels. However, as pixel values increase beyond 5, the FSIM begins to decline, dropping to 0.9398 at 10 pixels, 0.9215 at 15 pixels, and reaching its lowest value of 0.8359 at 20 pixels. This trend suggests that higher pixel values reduce similarity, likely due to a loss of fine details during processing.

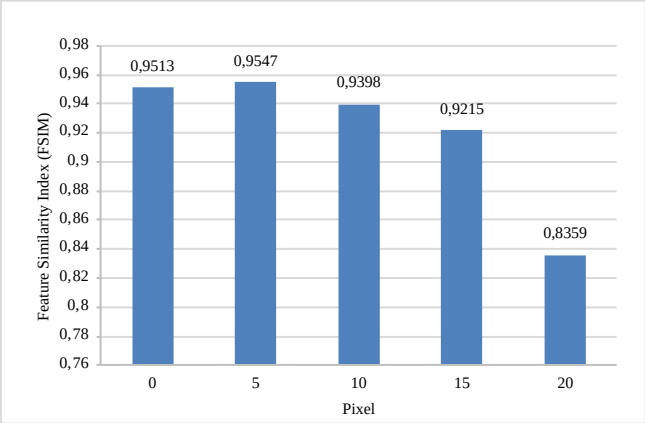

Fig. 8. Feature Similarity Index (FSIM).

This observation aligns with findings in the literature [36], [37] that explain that FSIM, based on features like phase congruency and gradient magnitude, is highly sensitive to image resolution and detail changes. Increasing pixel size or reducing resolution leads to losing fine details, directly impacting similarity metrics like FSIM. Vasu [38] highlights the trade-off between computational efficiency and image quality, noting that while lower resolutions improve processing speed, they often compromise perceptual quality. Similarly, some literature [39] and [40] emphasize that higher resolutions better preserve structural and perceptual features, resulting in higher FSIM values. Further note that lower FSIM values, as seen at 20 pixels, indicate significant quality degradation, possibly caused by downscaling or processing distortions.

6) Processing time: Fig. 9 shows the relationship between pixel values and processing time in seconds. The X-axis represents pixel values ranging from 0 to 20, while the Y-axis shows time in seconds. The data reveals a clear decreasing trend in processing time as pixel values increase. At 0 pixels, the time is the highest, approximately 3.097 seconds, while the lowest time, 2.5986 seconds, is observed at 20 pixels. The reduction in processing time is steeper between 0 and 10 pixels and becomes less pronounced at higher pixel values. This trend aligns with findings in the literature. The study in [41] explain that higher pixel counts typically increase processing time due to the larger data volume. However, optimizations like subsampling and dimensionality reduction can mitigate this issue, resulting in shorter processing times for larger pixel values. Similarly, the study in [42] highlights that reducing pixel density, such as through downscaling, enhances computational efficiency while maintaining adequate performance for applications like object detection. The study in [43] further notes that processing time reductions tend to plateau beyond a certain resolution threshold due to hardware and memory limitations. As emphasized by [44], balancing resolution and processing time is critical in real-time systems. Higher resolutions are only employed when necessary, as the exponential time costs outweigh the benefits of marginal improvements in detail.

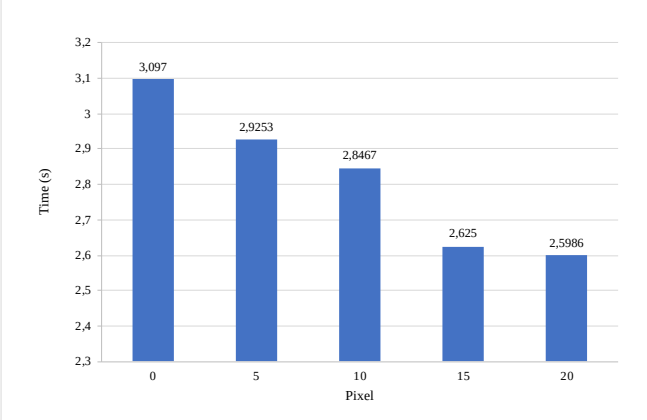

Fig. 9. Processing time.

Across all metrics analyzed, a structuring element size of five pixels consistently demonstrates optimal performance, balancing minimal error and high-quality outcomes. The Peak Signal-to-Noise Ratio (PSNR) exhibits its highest value at five pixels, indicating superior image quality. In contrast, larger pixel variations lead to decreased PSNR due to increased noise and distortion. Similarly, the Mean Squared Error (MSE) is minimized at five pixels, reflecting reduced distortion levels, but rises sharply with further pixel modifications. Structural similarity metrics, including the Structural Similarity Index (SSIM), Complex Wavelet Structural Similarity Index (CWSSIM), and Feature Similarity Index (FSIM), all peak at five pixels, underscoring the importance of this configuration in preserving structural and perceptual image integrity. Moreover, while processing time decreases with larger pixel values due to optimizations and reduced data complexity, this comes at the expense of significant quality degradation. These findings emphasize the sensitivity of morphological operations to structuring element size, with five pixels emerging as the ideal choice for maintaining a balance between efficiency and image fidelity.

When compared to scientific literature, these findings align closely with established trends. Research demonstrates that

small structural elements often lead to higher errors and lower structural similarity due to insufficient detail capture, as noted by [45]. Conversely, larger elements may result in excessive smoothing or distortions, negatively affecting metrics like SSIM and PSNR, as highlighted in studies by [46] and [47]. Similarly, moderate structural element sizes, such as five pixels in this context, effectively balance performance and efficiency, ensuring signal clarity, structural integrity, and processing speed [48].

B. Enhancement of Coastline Video Monitoring System Framework Using Structuring Element Morphological Operations

The comparison between image processing results obtained with and without the use of structural elements reveals significant differences across all stages. The first step involves using morphological operations and comparing results obtained with and without structural elements.

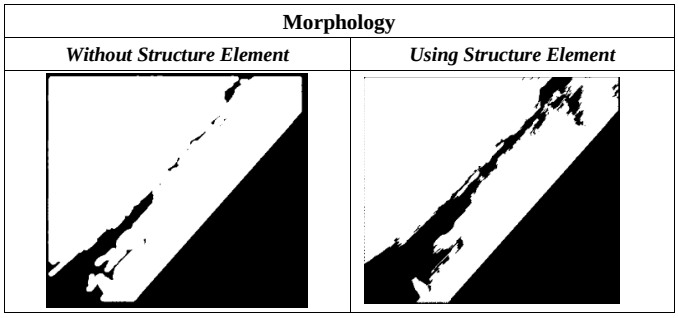

Fig. 10. Morphology comparison

From Fig. 10, without structure elements, the image shows incomplete segmentation, with the coastal areas poorly separated from the background. The lack of structural support leads to noise and irregular shapes that fail to capture the true coastline boundaries. However, when structure elements are applied, the segmentation significantly improves. Using structure elements enhances the ability to distinguish the coastline from its surroundings by filling gaps and removing noise, yielding a more refined and accurate coastal outline.

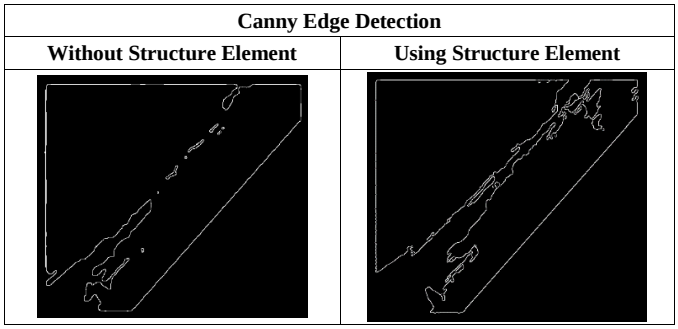

Fig. 11. Canny Edge Detection Comparison

The step continued with canny edge detection. The performance of the Canny edge detection algorithm (Fig. 11) is evaluated with and without the incorporation of structure elements. Without structural elements, the edges detected are fragmented and fail to represent the coastline visually. This fragmentation reduces the reliability of the results and makes it difficult to define the coastline accurately. By introducing structural elements, the continuity of the detected edges improves significantly, with the coastline appearing clearer and better connected.

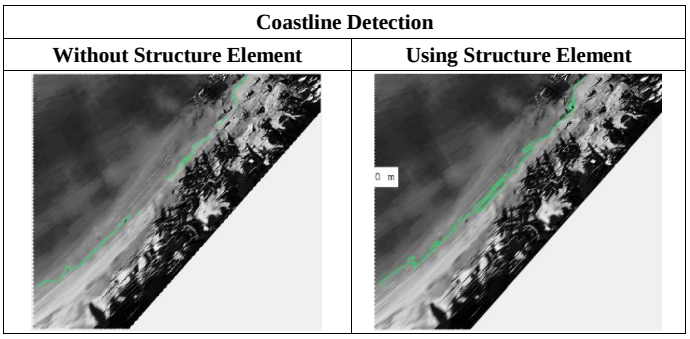

Fig. 12. Coastline detection comparison

The coastline detection results shown in Fig. 12 marked improvement when structure elements are used. Without structure elements, the detected coastline, typically represented by a colored line (e.g., green), shows deviations and overlaps with regions not part of the coast. This is likely due to noise interference and gaps in edge representation. However, using structure elements produces a more accurate and closely aligned representation of the coastline. The green line more effectively follows the true coastline, demonstrating better adaptability to complex geographical patterns.

The final comparison against ground truth data (Fig. 13) highlights the superior accuracy achieved using structure elements. Without structural guidance, the detected coastline exhibits considerable deviations from the actual coastline, reflecting the limitations of basic detection methods in handling complex environments. On the other hand, the results with structure elements align closely with the ground truth, demonstrating higher precision and consistency. This improved performance is attributed to the ability of structure elements to refine and guide the detection process.

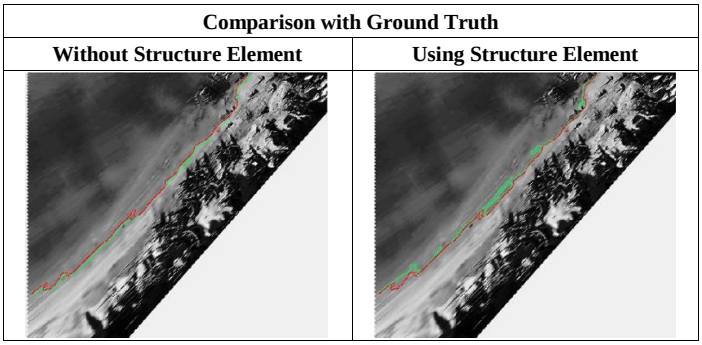

Fig. 13. Calibration with ground truth data comparison

C. Metric Performance of Coastline Video Monitoring System Framework Using Structuring Element Morphological Operations

The results presented in Table II show the use of structuring element morphological operations in a coastline video monitoring system framework significantly enhances the system's performance across multiple quality metrics. Specifically, the Peak Signal-to-Noise Ratio (PSNR) improved

by 9.3%, increasing from 24.7233 to 27.0245, and the Structural Similarity Index (SSIM) rose by 1.4%, from 0.9044 to 0.9171. Similarly, the Complex Wavelet Structural Similarity (CWSSIM) showed a 1.7% improvement, increasing from 0.9583 to 0.9749, while the Feature Similarity Index (FSIM) improved by 1.6%, rising from 0.9398 to 0.9547. Additionally, the processing time decreased slightly by 1.3%, from 2.9626 seconds to 2.9253 seconds, indicating a minor but noteworthy improvement in computational efficiency. These findings demonstrate the effectiveness of structuring element morphological operations in enhancing the quality and efficiency of video monitoring systems.

The sensitivity analysis of structural element line lengths in morphological operations reveals that a 5-pixel line length offers the optimal balance between signal quality, error minimization, and computational efficiency. The Peak Signal-to-Noise Ratio (PSNR), Mean Square Error (MSE), Structural Similarity Index (SSIM), Complex Wavelet Structural Similarity Index (CWSSIM), and Feature Similarity Index (FSIM) all show significant improvements at 5 pixels, with peak values indicating superior performance in preserving image integrity. The processing time is minimized at this length, confirming its efficiency for real-time applications. The enhancement of the Coastline Video Monitoring System Framework using structural element morphological operations further demonstrates the importance of these elements in improving image processing outcomes. Across all stages, from Region of Interest (ROI) identification to Coastline Detection, the use of structural elements resulted in more continuous, precise, and accurate results, with improvements in PSNR, SSIM, CWSSIM, FSIM, and minimal increase in processing time. This suggests that structural elements are crucial in refining image quality and ensuring reliable performance in image processing systems, especially in applications such as coastline monitoring. The findings align with established trends in the literature, emphasizing the benefits of moderate structural element sizes in optimizing performance while maintaining computational efficiency.

TABLE II. METRIC PERFORMANCE OF COASTLINE VIDEO MONITORING SYSTEM FRAMEWORK USING STRUCTURING ELEMENT MORPHOLOGICAL OPERATIONS

Parameter	Without Structure Element	Using Structure Element	Enhancement
PNSR	24,7233	27,0245	9,3%
SSIM	0,9044	0,9171	1,4%
CWSSIM	0,9583	0,9749	1,7%
FSIM	0,9398	0,9547	1,6%
Time	2,9626	2,9253	-1,3%

IV. CONCLUSION

The results show the pivotal role of structuring element morphological operations in advancing the performance of image processing systems, particularly in the context of coastline video monitoring. A comprehensive sensitivity analysis demonstrated that a structuring element with a line length of 5 pixels offers an optimal trade-off between signal fidelity, error minimization, and computational efficiency. Key metrics such as Peak Signal-to-Noise Ratio (PSNR), Structural Similarity Index (SSIM), Complex Wavelet Structural Similarity Index (CWSSIM), and Feature Similarity Index (FSIM) consistently achieved their highest values at this configuration, reflecting significant improvements in both perceptual and structural image quality. Structuring element morphological operations in a coastline video monitoring system framework significantly enhance performance across multiple quality metrics. Specifically, the Peak Signal-to-Noise Ratio (PSNR) improved by 9.3%, increasing from 24.7233 to 27.0245, and the Structural Similarity Index (SSIM) rose by 1.4%, from 0.9044 to 0.9171. Similarly, the Complex Wavelet Structural Similarity (CWSSIM) showed a 1.7% improvement, increasing from 0.9583 to 0.9749, while the Feature Similarity Index (FSIM) improved by 1.6%, rising from 0.9398 to 0.9547. Additionally, the processing time decreased slightly by 1.3%, from 2.9626 seconds to 2.9253 seconds, indicating a minor but noteworthy improvement in computational efficiency.

REFERENCES

[1] B. El Mahrad, A. Newton, J. D. Icely, I. Kacimi, S. Abalansa, and M. Snoussi, ‘Contribution of remote sensing technologies to a holistic coastal and marine environmental management framework: A review’, Remote Sens (Basel), vol. 12, no. 14, 2020, doi: 10.3390/rs12142313.

[2] Z. Yang et al., ‘UAV remote sensing applications in marine monitoring: Knowledge visualization and review’, 2022. doi: 10.1016/j.scitotenv.2022.155939.

[3] E. Politi, S. K. Paterson, R. Scarrott, E. Tuohy, C. O’mahony, and W. C. A. Cámaro-García, ‘Earth observation applications for coastal sustainability: Potential and challenges for implementation’, 2019. doi: 10.1139/anc-2018-0015.

[4] S. Vitousek, D. Buscombe, K. Vos, P. L. Barnard, A. C. Ritchie, and J. A. Warrick, ‘The future of coastal monitoring through satellite remote sensing’, Cambridge Prisms: Coastal Futures, vol. 1, 2023, doi: 10.1017/cft.2022.4.

[5] D. Apostolopoulos and K. Nikolakopoulos, ‘A review and meta-analysis of remote sensing data, GIS methods, materials and indices used for monitoring the coastline evolution over the last twenty years’, 2021. doi: 10.1080/22797254.2021.1904293.

[6] Y. L. S. Tsai, ‘Monitoring 23-year of shoreline changes of the Zengwun Estuary in Southern Taiwan using time-series Landsat data and edge detection techniques’, Science of the Total Environment, vol. 839, 2022, doi: 10.1016/j.scitotenv.2022.156310.

[7] B. Laignel et al., ‘Observation of the Coastal Areas, Estuaries and Deltas from Space’, 2023. doi: 10.1007/s10712-022-09757-6.

[8] B. M. S. Rani, V. D. Majety, C. S. Pittala, V. Vijay, K. S. Sandeep, and S. Kiran, ‘Road identification through efficient edge segmentation based on morphological operations’, Traitement du Signal, vol. 38, no. 5, 2021, doi: 10.18280/ts.380526.

[9] J. Jing, S. Liu, G. Wang, W. Zhang, and C. Sun, ‘Recent advances on image edge detection: A comprehensive review’, Neurocomputing, vol. 503, 2022, doi: 10.1016/j.neucom.2022.06.083.

[10] S. S. Chouhan, A. Kaul, and U. P. Singh, ‘Image Segmentation Using Computational Intelligence Techniques: Review’, Archives of Computational Methods in Engineering, vol. 26, no. 3, 2019, doi: 10.1007/s11831-018-9257-4.

[11] P. Kaur and J. Singh, ‘A Study on the Effect of Gaussian Noise on PSNR Value for Digital Images’, International Journal of Computer and Electrical Engineering, 2011, doi: 10.7763/ijcee.2011.v3.334.

[12] M. Ajay Kumar, N. Sravan Goud, R. Sreeram, and R. Gnana Prasuna, ‘Image Processing based on Adaptive Morphological Techniques’, in 2019 International Conference on Emerging Trends in Science and Engineering, ICESE 2019, 2019. doi: 10.1109/ICESE46178.2019.9194641.

[13] Y. Shen, F. Y. Shih, X. Zhong, and I. C. Chang, 'Deep Morphological Neural Networks', Intern J Pattern Recognit Artif Intell, vol. 36, no. 12, 2022, doi: 10.1142/S0218001422520231.

[14] K. Nogueira, J. Chanussot, M. D. Mura, and J. A. D. Santos, 'An Introduction to Deep Morphological Networks', IEEE Access, vol. 9, 2021, doi: 10.1109/ACCESS.2021.3104405.

[15] I. M. O. Widyantara, I. M. D. A. Putra, and I. B. P. Adnyana, 'COVIMOS: A Coastal Video Monitoring System', Journal of Electrical, Electronics and Informatics, vol. 1, no. 1, 2017, doi: 10.24843/jeei.2017.v01.i01.p01.

[16] Y. S. Chang, J. Y. Jin, W. M. Jeong, C. H. Kim, and J. D. Do, 'Video monitoring of shoreline positions in Hujeong Beach, Korea', Applied Sciences (Switzerland), vol. 9, no. 23, 2019, doi: 10.3390/app9234984.

[17] P. Upadhyay and J. K. Chhabra, 'Kapur's entropy based optimal multilevel image segmentation using Crow Search Algorithm', Appl Soft Comput, vol. 97, 2020, doi: 10.1016/j.asoc.2019.105522.

[18] R. Singh, P. Agarwal, M. Kashyap, and M. Bhattacharya, 'Kapur's and Otsu's based optimal multilevel image thresholding using social spider and firefly algorithm', in International Conference on Communication and Signal Processing, ICCSP 2016, 2016. doi: 10.1109/ICCSP.2016.7754088.

[19] A. K. Bhandari, V. K. Singh, A. Kumar, and G. K. Singh, 'Cuckoo search algorithm and wind driven optimization based study of satellite image segmentation for multilevel thresholding using Kapur's entropy', Expert Syst Appl, vol. 41, no. 7, 2014, doi: 10.1016/j.eswa.2013.10.059.

[20] S. Saremi, S. Mirjalili, and A. Lewis, 'Grasshopper Optimisation Algorithm: Theory and application', Advances in Engineering Software, vol. 105, 2017, doi: 10.1016/j.advengsoft.2017.01.004.

[21] Y. Meraihi, A. B. Gabis, S. Mirjalili, and A. Ramdane-Cherif, 'Grasshopper optimization algorithm: Theory, variants, and applications', IEEE Access, vol. 9, 2021, doi: 10.1109/ACCESS.2021.3067597.

[22] A. A. Ewees, M. Abd Elaziz, and E. H. Houssein, 'Improved grasshopper optimization algorithm using opposition-based learning', Expert Syst Appl, vol. 112, 2018, doi: 10.1016/j.eswa.2018.06.023.

[23] H. Liu and K. C. Jezek, 'Automated extraction of coastline from satellite imagery by integrating Canny edge detection and locally adaptive thresholding methods', Int J Remote Sens, vol. 25, no. 5, 2004, doi: 10.1080/0143116031000139890.

[24] X. Hu and Y. Wang, 'Monitoring coastline variations in the Pearl River Estuary from 1978 to 2018 by integrating Canny edge detection and Otsu methods using long time series Landsat dataset', Catena (Amst), vol. 209, 2022, doi: 10.1016/j.catena.2021.105840.

[25] I. M. O. Widyantara, N. M. Ary Esta Dewi Wirastuti, I. M. D. P. Asana, and I. B. P. Adnyana, 'Gamma correction-based image enhancement and canny edge detection for shoreline extraction from coastal imagery', in Proceedings - 2017 1st International Conference on Informatics and Computational Sciences, ICICoS 2017, 2017. doi: 10.1109/ICICOS.2017.8276331.

[26] B. Devkota, A. Alsadoon, P. W. C. Prasad, A. K. Singh, and A. Elchouemi, 'Image Segmentation for Early Stage Brain Tumor Detection using Mathematical Morphological Reconstruction', in Procedia Computer Science, 2018. doi: 10.1016/j.procs.2017.12.017.

[27] N. D. Hoang and Q. L. Nguyen, 'Metaheuristic optimized edge detection for recognition of concrete wall cracks: A comparative study on the performances of Roberts, Prewitt, Canny, and Sobel algorithms', Advances in Civil Engineering, vol. 2018, 2018, doi: 10.1155/2018/7163580.

[28] K. Goel, M. Sehrawat, and A. Agarwal, 'Finding the optimal threshold values for edge detection of digital images & comparing among Bacterial Foraging Algorithm, canny and Sobel Edge Detector', in Proceeding - IEEE International Conference on Computing, Communication and Automation, ICCCA 2017, 2017. doi: 10.1109/CCAA.2017.8229955.

[29] M. Elad, B. Kawar, and G. Vaksman, 'Image Denoising: The Deep Learning Revolution and Beyond---A Survey Paper', SIAM J Imaging Sci, vol. 16, no. 3, 2023, doi: 10.1137/23M1545859.

[30] C. A. Duarte-Salazar, andres E. Castro-Ospina, M. a. Becerra, and E. Delgado-Trejos, 'Speckle Noise Reduction in Ultrasound Images for Improving the Metrological Evaluation of Biomedical applications: an Overview', IEEE Access, vol. 8, 2020, doi: 10.1109/aCCESS.2020.2967178.

[31] W. Yan, G. Yue, Y. Fang, H. Chen, C. Tang, and G. Jiang, 'Perceptual objective quality assessment of stereoscopic stitched images', Signal Processing, vol. 172, 2020, doi: 10.1016/j.sigpro.2020.107541.

[32] M. G. Albanesi, R. Amadeo, S. Bertoluzza, and G. Maggi, 'A New Class of Wavelet-Based Metrics for Image Similarity Assessment', J Math Imaging Vis, vol. 60, no. 1, 2018, doi: 10.1007/s10851-017-0745-1.

[33] V. Mudeng, M. Kim, and S. W. Choe, 'Prospects of Structural Similarity Index for Medical Image Analysis', 2022. doi: 10.3390/app12083754.

[34] C. G. Rodríguez-Pulecio, H. D. Benítez-Restrepo, and A. C. Bovik, 'Making long-wave infrared face recognition robust against image quality degradations', Quant Infrared Thermogr J, vol. 16, no. 3–4, 2019, doi: 10.1080/17686733.2019.1579020.

[35] K. Ganesh and C. M. Patil, 'Performance Analysis of CWSSIM Video Quality Metric with Different Window Size on LIVE Database', in International Conference on Current Trends in Computer, Electrical, Electronics and Communication, CTCEEC 2017, 2018. doi: 10.1109/CTCEEC.2017.8455129.

[36] Z. Ye et al., 'Illumination-Robust Subpixel Fourier-Based Image Correlation Methods Based on Phase Congruency', IEEE Transactions on Geoscience and Remote Sensing, vol. 57, no. 4, 2019, doi: 10.1109/TGRS.2018.2870422.

[37] C. Chen and X. Mou, 'Phase congruency based on derivatives of circular symmetric Gaussian function: an efficient feature map for image quality assessment', EURASIP J Image Video Process, vol. 2023, no. 1, 2023, doi: 10.1186/s13640-023-00611-2.

[38] S. Vasu, N. Thekke Madam, and A. N. Rajagopalan, 'Analyzing perception-distortion tradeoff using enhanced perceptual super-resolution network', in Lecture Notes in Computer Science (including subseries Lecture Notes in Artificial Intelligence and Lecture Notes in Bioinformatics), 2019. doi: 10.1007/978-3-030-11021-5_8.

[39] Z. Wang, A. C. Bovik, and H. R. Sheikh, 'Structural similarity based image quality assessment', in Digital Video Image Quality and Perceptual Coding, 2017. doi: 10.1201/9781420027822-7.

[40] K. Gu, L. Li, H. Lu, X. Min, and W. Lin, 'A fast reliable image quality predictor by fusing micro- and macro-structures', IEEE Transactions on Industrial Electronics, vol. 64, no. 5, 2017, doi: 10.1109/TIE.2017.2652339.

[41] M. Garcia-Sciveres and N. Wermes, 'A review of advances in pixel detectors for experiments with high rate and radiation', 2018. doi: 10.1088/1361-6633/aab064.

[42] T. Hoeser and C. Kuenzer, 'Object detection and image segmentation with deep learning on Earth observation data: A review-part I: Evolution and recent trends', 2020. doi: 10.3390/rs12101667.

[43] G. Denes, K. Maruszczyk, G. Ash, and R. K. Mantiuk, 'Temporal Resolution Multiplexing: Exploiting the limitations of spatio-temporal vision for more efficient VR rendering', IEEE Trans Vis Comput Graph, vol. 25, no. 5, 2019, doi: 10.1109/TVCG.2019.2898741.

[44] L. Yan, Y. Qin, and J. Chen, 'Scale-Balanced Real-Time Object Detection With Varying Input-Image Resolution', IEEE Transactions on Circuits and Systems for Video Technology, vol. 33, no. 1, 2023, doi: 10.1109/TCSVT.2022.3198329.

[45] P. Bergmann, S. Löwe, M. Fauser, D. Sattlegger, and C. Steger, 'Improving unsupervised defect segmentation by applying structural similarity to autoencoders', in VISIGRAPP 2019 - Proceedings of the 14th International Joint Conference on Computer Vision, Imaging and Computer Graphics Theory and Applications, 2019. doi: 10.5220/0007364503720380.

[46] M. Azam and M. Nouman, 'Evaluation of Image Support Resolution Deep Learning Technique based on PSNR Value', KIET Journal of Computing and Information Sciences, vol. 6, no. 1, 2022, doi: 10.51153/kjcis.v6i1.160.

[47] B. Maiseli, 'Nonlinear anisotropic diffusion methods for image denoising problems: Challenges and future research opportunities', Array, vol. 17, 2023, doi: 10.1016/j.array.2022.100265.

[48] Y. Liu, Z. Zhang, X. Liu, L. Wang, and X. Xia, 'Efficient image segmentation based on deep learning for mineral image classification', Advanced Powder Technology, vol. 32, no. 10, 2021, doi: 10.1016/j.apt.2021.08.038.